

IMECE2002-33682

MICROCHANNEL FLOW MEASUREMENT USING MICRO PARTICLE IMAGE VELOCIMETRY

Sang-Youp Lee

School of Mechanical Engineering, Purdue University
Microfluidics Laboratory
Rm. 338, Potter Engineering Center
West Lafayette, IN 47907
Ph: 765-494-7057, Fax: 765-494-0539
Email: leesy1@ecn.purdue.edu

Steven T. Wereley

School of Mechanical Engineering, Purdue University
Microfluidics Laboratory
Rm. 175, 1288 Potter Engineering Center
West Lafayette, IN 47907
Ph: 765-494-5624, Fax: 765-494-0539
Email: wereley@purdue.edu

Lichuan Gui

School of Mechanical Engineering, Purdue University
Microfluidics Laboratory
Rm. 338, Potter Engineering Center
West Lafayette, IN 47907
Ph: 765-494-7057, Fax: 765-494-0539
Email: guil@purdue.edu

Weilin Qu

School of Mechanical Engineering, Purdue University
Boiling and Two-Phase Flow Laboratory
Rm. 191, 1288 Mechanical Engineering
West Lafayette, IN 47907
Ph: 765-494-5634, Fax: 765-494-0539
Email: quw@purdue.edu

Issam Mudawar

School of Mechanical Engineering, Purdue University
Boiling and Two-Phase Flow Laboratory
Rm. 173, 1288 Mechanical Engineering
West Lafayette, IN 47907
Ph: 765-494-5705, Fax: 765-494-0539
Email: mudawar@ecn.purdue.edu

ABSTRACT

Since microfabrication techniques are typically planar processes, microchannel flows typically have significant predevelopment due to the upstream reservoir having the same height as the microchannel. The main concerns of the current study are categorized into finding the effects of typical microchannel geometry on the velocity entrance length in the laminar flow regime and providing the turbulence transitional Reynolds number range using the details of the velocity profile rather than global measurements of pressure drop. A rectangular micro-channel of aspect ratio ~ 2.65 and the hydraulic diameter $380\mu\text{m}$ was used in this study. Micro particle image velocimetry measurement was performed to measure the velocity profiles. The entrance length is reduced about 45% and the transitional velocity profile is measured at $Re=2900$. The velocity profiles do not show deviation from the fully developed laminar flow profiles up to $Re=2100$. Related to the flow transition, the close resemblance between the correlation function peak broadening and the turbulence intensity is observed.

INTRODUCTION

In studies of duct flow, entrance effects and laminar to turbulent transition are two of the most fundamental and important subjects. These features are important design parameters in practical applications because properties, such as pressure gradient, wall shear stress and heat transfer coefficient, show the different behaviors according to both the flow regime, *i.e.* laminar or turbulent, and the flow region, *i.e.* the hydrodynamic developing region (the entrance region) or the developed region. The pressure drop in the developing region exceeds its value in the fully developed region because it must overcome the wall shear and increase the flow momentum.

As channel flow applications have been extended to the small scale, the microchannels for various purposes have been constructed using microfabrication techniques. Microchannels for electronics cooling or that take advantage of the high surface to volume ratio are typical applications. Tuckermann and Pease [1] fabricated a microchannel array on the backside of VLSI (Very Large Scale Integrated) circuit for cooling purposes and showed that cooling performance was significantly increased.

Analytical and experimental work to understand the flow physics in rectangular macroscale channels were performed extensively in 60's and 70's.[2-12] Most works were devoted to finding both the pressure drop and the velocity profiles in the entrance region, along with the entrance length. On the other hand, specific analyses of the microchannel flow have been focused on the size effects on the friction factor and the flow transition, since the Wu and Little[13] observed the abnormal behavior in the microchannel flow. Later, deviations from conventional hydrodynamic observations were found by several experimenters but the results are not conclusive yet.[13-16]

The velocity profiles in rectangular channels are somewhat more complicated than those of circular channels. In a rectangular channel, four boundary layers begin at the each wall like the boundary layer growth on the flat plate and merge at some distance downstream. The hydrodynamic entrance region is where the velocity boundary layer, the pressure gradient, and wall shear stress are developing. The entrance length is the distance to attain their constant conditions (*i.e.* fully developed conditions). The definition of the entrance length can be made based on the pressure gradient as well as the velocity profile. The pressure entrance length is usually somewhat shorter than the velocity entrance length.[5] To decide the precise entrance length is difficult because of the asymptotic approaches of the three variables to their constant conditions.[25] For engineering purposes, the entrance length is defined, in general, as the axial distance required for the centerline velocity to reach 99% of the fully developed velocity. There exist several correlations for entrance length estimates.[24]

The uniform velocity profile, typically assumed at the entrance when viscous fluid is entering a duct, is seldom achieved in practice because the flow development, taking place in the contraction section, is unavoidable.[5] Further, the velocity overshoot caused by the abrupt change of the velocity at the wall and the sharp turn of the velocity at the entrance make it also difficult to have the uniform inlet velocity profiles. [3,6,8,10,11,23]

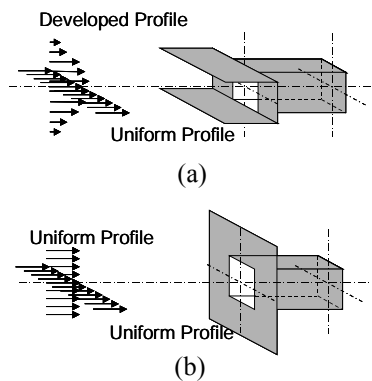


Fig. 1. Comparison of Entering Flow Conditions

Since most microchannels are fabricated using planar processes, the height of the reservoir upstream of the microchannel entrance, *i.e.* the distance between the top and bottom walls, is same as the height of the microchannel.

Therefore, the velocity profile at the entrance of the microchannel is a combination of the developed vertical velocity profile and the uniform horizontal velocity profile rather than simply uniform velocity profile as is assumed in macroscopic cases. This altered inlet condition may reduce both the pressure loss at the entry region and the entrance length.

Size effects on the microchannel flow have been observed in previous experiments.[13-15] The results from these early works, based on the qualitative bulk flow measurements, showed deviation from conventional results in the friction constant, fRe , and in the exponent of Reynolds number, which determines the rate of decrease of friction factor in the laminar region of the Moody chart. Further, the trend of the friction factor showed transition at low Reynolds number ranges. Sharp *et al.*[16] performed both bulk flow measurement and the quantitative flow measurement, micro-PIV, in a circular microchannel. Though there were slight deviations from laminar flow theory for Re higher than 1500-1800, both results agree with conventional theory up to $Re=1500-1800$. The very large pressure gradient necessary to move flows in small channels was proposed for the reason of the deviation rather than large surface roughness or early transition.

In the current study, the micro particle image velocimetry (μ PIV) was used for the velocity profile measurement. Also, an attempt to relate the μ PIV correlation analysis to the degree of the turbulence was made. The results of the velocity profiles in the entrance region show that the planar entrance geometry of the typical microchannel shortens the entrance length by 45%. The fully developed velocity profiles show good agreement with the analytical solution up to $Re=2100$. Transitional behavior of the velocity profile was found at $Re=2900$, which agrees with the conventional macroscopic results. The close resemblance of correlation function peak broadening with the turbulence intensity has been observed.

NOMENCLATURE

| | |
|-----------|----------------------------------|
| L_e | Entrance length |
| C_e | Dimensionless entrance length |
| Re | Reynolds number = UD_h/ν |
| f | Friction factor |
| D_h | Hydraulic diameter = $2WH/(W+H)$ |
| x | Axial distance from the entrance |
| A_c | Cross-sectional area = WH |
| P | Perimeter = $2(W+H)$ |
| α | Aspect ratio = H/W |
| W | Channel width |
| H | Channel height |
| U | Normalized velocity |
| u | Velocity fluctuation |
| U_{max} | Local maximum velocity |
| U_{CL} | Centerline velocity |
| U_{avg} | Mean velocity |
| N | Number of images |

Subscript

| | |
|------|----------------------|
| fd | Fully developed |
| 1 | Streamwise direction |
| o | Channel center |

EXPERIMENTAL APPARATUS AND PROCEDURE

Micro Particle Image Velocimetry System

Figure 2. shows a schematic of the μ PIV system[17,19] used to make the measurements. A two cavity frequency-doubled Nd:YAG laser (*New Wave Inc.*) is used for the illumination. The wavelength and the pulse width are $532nm$ and about $3\sim 5ns$, respectively. The laser beam is delivered into the inverted epi-fluorescent microscope (*Nikon, TE200*) through the beam expander assembly, which is located between the laser aperture and the microscope back aperture. This beam expander assembly is carefully designed for laser beam to have similar characteristics to the original mercury lamp. A negative and a positive lens in a Galilean telescope arrangement are used to expand the beam and a 5° diffuser is located between two lenses to disorder the spatial coherence of the laser beam so that laser focal points do not damage internal optics. The laser beam is guided to the flow field of the microchannel device by passing through an epi-fluorescence filter cube and an objective lens. The filter cube, located below the objective lens, is an assembly of the exciter (green filter), emitter (red filter), and a dichroic mirror. Because the dichroic mirror only transmits light in the range $> 610nm$, the beam is redirected to the objective lens. The beam coming out the objective lens illuminates a large volume of fluid and the seeding particles suspending in that volume. The particle density must be considered carefully in μ PIV, because the background noise keeps increasing as the particle density increases, while the particle image intensity remains about same value.[20] Since the microchannel in the current study has a large depth ($\sim 690\mu m$), the ratio of the out-of-focus volume to focused volume is also large. The particle density is optimized to be 0.038% (by volume) by balancing the valid detection rate and the background noises from out-of-plane particles.

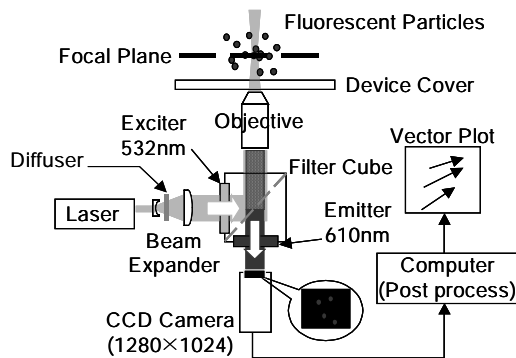


Fig. 2. The schematic of μ PIV system

Fluorescent particles (*Duke Scientific Co.*) are used for flow seeding and their size is $\sim 1\mu m$ in diameter. The fluorescent particles absorb the illuminating laser beam ($\lambda \sim 532nm$, green) and emit a longer wavelength ($\lambda \sim 610nm$, red). The signal from the measurement region includes the emitted light from both in-focus and out-of-focus particles, and the reflection from the background. The reflection from background is eliminated by the emitter filter and the dichroic mirror while both the focused

and unfocused particle images are imaged on the interline transfer CCD camera (*LaVision, Inc.*). After a specified time delay Δt the same process as described above is performed to acquire the second image frame for the cross correlation based interrogation.

Microchannel Fabrication

The microchannel used in the experiment was fabricated from transparent acrylic. Figure 3(a) shows the fabrication procedure. The microchannel groove and the cover plate are made using the conventional machining, a precision sawing technique. The $1.6mm$ thick cover plate is laminated with a $25.4\mu m$ thick pressure sensitive adhesive layer (*Adhesive Research Inc.*) having an optical transmission rate over 95%. This plate is bonded on top of the microchannel groove. Further, this bonded piece is compressed by an external clamp to ensure that the channel is leak proof.

To assure that the microchannel has sufficient length to fully develop, a long microchannel of $120mm$ is fabricated. The dimension of the assembled microchannel is measured using the microscope. Conventional machining at these small length scales yields indefinite boundaries and, therefore, the variation of the microchannel dimension is relatively large. The average dimension is calculated as $\sim 260 \times 690\mu m^2$.

Figure 3(b) shows the completed microchannel structure. The two deep reservoirs or plenums leading to the shallow plenums are built at both ends of the microchannel to ensure even distribution of the flow.

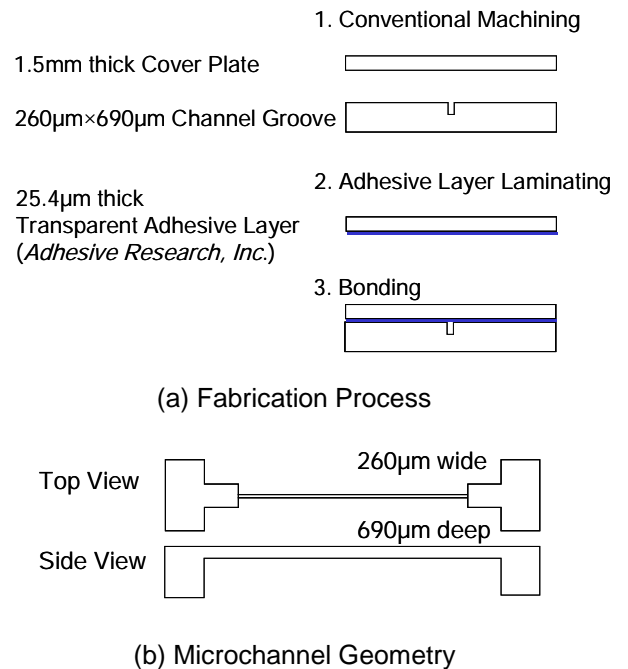


Fig. 3. Fabrication procedure and Microchannel geometry

Fluid Supply System

Figure 4. shows a schematic of the fluid supply system. Deionized water is used for the working fluid. A variable speed gear pump is used to pump the fluid through the channel. The

volume flow rate is measured using high and low range rotameters. For the fine control of the flow rate, a by-pass loop is installed so that a portion of the water can return to the reservoir without passing through the microchannel. To monitor the pressures of the exiting flow from the pump and returning flow to the reservoir, two pressure gauges are installed immediately downstream of the pump and the test module. Water temperature is measured both upstream and downstream of the test module using thermocouple probes. The rotameters were calibrated at several different water temperatures using the standard weight versus time method. The accuracy for the flow rate measurement was determined to be better than 4%.

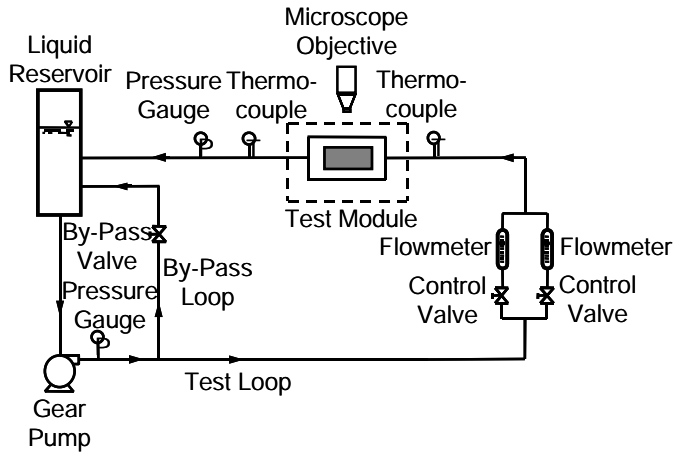


Fig. 4. Fluid supply system

Procedure

Experiments were performed at four Reynolds numbers, $Re=250, 1020, 1800, 2100$, all of which could be expected to exhibit laminar behavior according to macroscale theory. A fifth Reynolds number was chosen ($Re=2900$) at which the flow was expected to be non-laminar (transitioning to turbulence). Images were acquired every $1cm$ along the microchannel for the four lower Reynolds numbers and every $10cm$ for $Re=2900$. At each measurement position, 100 pairs of images were taken. Optical access was available from the narrow side (*i.e.*, $260\mu m$ in width and $690\mu m$ in depth) of microchannel. The focal plane was adjusted so that it was at the middle of the microchannel depth.

The images showed poor quality for several reasons. First, because the cover plate is relatively thicker than the normal microscope cover slip thickness ($\sim 0.17mm$), the experiment was performed with low numerical aperture lenses, which means low light gathering power. Second, because of the large volume illuminated depth, high background noise is introduced to the images. Finally, the image quality near the wall was poor because the microchannel walls behave like an aperture reducing the amount of light reaching the camera.

The evaluation accuracy from the poor quality images was enhanced using the μPIV image filter and the average correlation algorithm. Because the images acquired using μPIV had the high frequency random noise (*i.e.* single pixel noise) and low frequency background noise, it was difficult to identify the evaluated correlation peaks. The μPIV image filter reduces

the evaluation errors caused by both high and low frequency noises so that clear correlation peak can be found.[23] On the other hand, the averaged correlation method increases the signal to noise ratio and reduces missing vectors.[18]

The velocity was measured every $1cm$ along the microchannel, 13 different positions in total. The field of view of a measurement position was about $428\mu m \times 343\mu m$ for a $20\times$ objective lens. Using interrogation windows measuring 8×16 pixels and 16×16 pixels, 77 velocity profiles are evaluated in each measurement position.

RESULTS AND DISCUSSTION

Entrance Length Measurement

In the macrochannel analysis, it is well known that the entrance length, L_e , is proportional to the tube diameter D and to the Reynolds number for laminar flow above $Re=100$.

$$L_e \approx C_e(D Re_D) \quad (1)$$

For noncircular ducts, the hydraulic diameter approximation can be applied to replace tube diameter, where the hydraulic diameter is defined as

$$D_h = \frac{4A_c}{P} = \frac{4ab}{2(a+b)} \quad (2)$$

A_c and P are the area of cross section and the perimeter, respectively, and a and b are the lengths of each side of the rectangular channel. The dimensionless entrance length, C_e , of ~ 0.06 is the accepted correlation.[24]

To represent the velocity profile at each measurement position, the velocity profiles were averaged in streamwise direction and normalized. The velocity was normalized with the maximum (centerline) velocity while the position was normalized the channel width.

In Fig. 5., the averaged and normalized velocity profiles at each position were overlapped to compare the velocity profiles along the channel at a given Reynolds number. The profiles from $1cm$ downstream to where the flow seems fully developed are plotted. The mean value and standard deviation of velocities in the fully developed region were calculated and error bars of two standard deviations were added to the plot.

For $Re=250$, see Fig. 5(a), velocity profiles up to $8cm$ downstream are overlapped. They all overlap within the two standard deviations. The flow seems already fully developed before the flow reaches $1cm$ downstream.

Fig. 5(b). shows velocity profiles up to $7cm$ downstream for $Re=1020$. To study more closely the velocity development between the inlet and $1cm$ downstream, extra measurement positions of $0.2cm$ increment were selected. The velocity profiles of 0.2 and $0.6cm$ are clearly deviated from the rest of profiles. Though the profiles from $1cm$ on show very close agreement with the rest of profiles, it is somewhat difficult to decide whether flow is fully developed. Without consideration of the entrance condition of present experiment, the entrance length estimate from Eq. (1). gives $L_e \approx 2.3cm$. A simple comparison of the conventional result with the Fig. 5(b) shows the entrance length becomes shorter due to the entrance effect.

As the flow rate increases, the developing region extends farther downstream than the early two low Reynolds number cases. Fig. 5(c) and (d) show that the velocity profiles at 1 and 2cm downstream are still approaching to the fully developed profile. Both flows finish their development between 2 and 3cm downstream but, from the comparison the deviations of the profiles of 2cm downstream from the rest of profiles, the case of Re=1800 shows somewhat faster development. The entrance lengths between 2 and 3cm downstream for both Re=1800 and Re=2100 again show a large difference from the conventional entrance length estimates of $L_e \approx 4.1\text{cm}$ and $L_e \approx 4.8\text{cm}$, respectively.

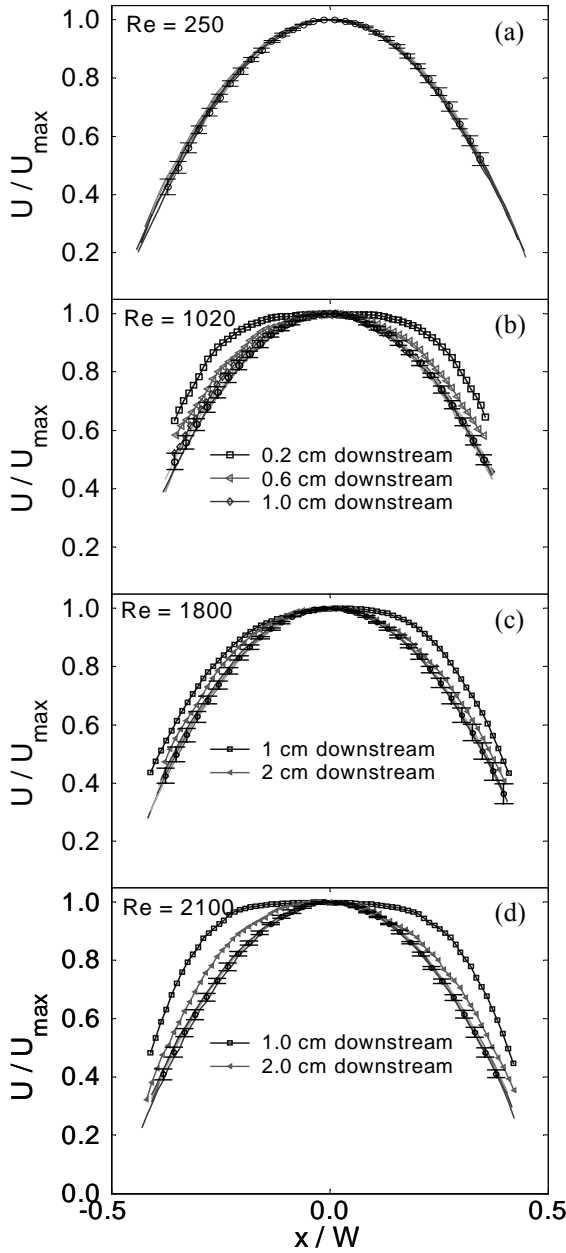


Fig. 5. Velocity profiles at various Reynolds numbers.

The centerline velocity development was considered for a more quantitative entrance length estimation. For a given aspect ratio, the developing velocity field can be described as a function of the dimensionless cross section coordinates and dimensionless axial coordinate as [5]

$$\frac{U}{U_{avg}} = fct\left(\frac{x}{a}, \frac{y}{b}, \frac{z/D_h}{Re}\right) \quad (3)$$

For the centerline velocity field, the velocity field is reduced to the function of dimensionless axial coordinate only.

$$\frac{U_{cl}}{U_{avg}} = fct\left(\frac{z/D_h}{Re}\right) \quad (4)$$

Similar to the extraction of the velocity profiles, the centerline velocities from each of the velocity profiles at a measurement position are averaged to calculate the centerline velocity at that measurement position. The averaged centerline velocities are non-dimensionalized using the average velocity, which is measured using the flowmeter.

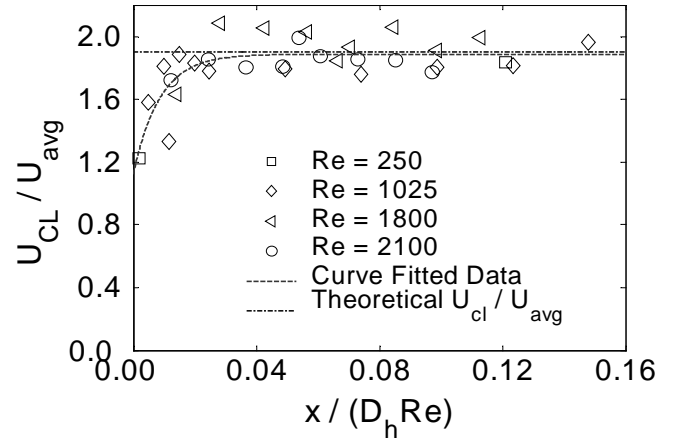


Fig. 6. The centerline velocity along the channel

Figure 6 shows the dimensionless centerline velocity development for all Reynolds number regimes. The fluctuation of the averaged centerline velocities is due to the experimental uncertainties such as microchannel dimensional uncertainty, hysteresis effects from the gear pump, and the rotameter read out errors. An exponential decay function is used to curve fit the centerline velocity data.

$$\frac{U_{cl}}{U_{avg}} = \left(\frac{U_{cl}}{U_{avg}}\right)_{fd} - A \exp\left(-B \frac{x/D_h}{Re}\right) \quad (5)$$

In this fitting function, care should be taken to decide the dimensionless centerline velocity in the fully developed region, $(U_{cl}/U_{avg})_{fd}$, because it changes the calculated entrance length drastically. In the current study, $(U_{cl}/U_{avg})_{fd}$ is found as the mean value of dimensionless centerline velocities, U_{cl}/U_{avg} , in the range of $(x/D_h)/Re > 0.06$, where flow is certainly fully developed according to conventional theory. The theoretical

dimensionless centerline velocity in the fully developed region, $(U_{CL}/U_{avg})_{fd}$, is about 1.9[24] and the fitting curve shows the criteria of $(x/D_h)/Re > 0.06$ is reasonable. By setting the centerline velocity equal to 99% of the fully developed velocity, the dimensionless entrance length is found to be ~ 0.033 . The calculated entrance length using $C_e = 0.033$ is tabulated in Table 1.

Table 1. Calculated entrance length

| Re | 250 | 1020 | 1800 | 2100 |
|------------|------|-------|-------|-------|
| $L_e [mm]$ | 3.14 | 12.85 | 22.57 | 26.33 |

Transition to Turbulence

To check the transitional Reynolds number range, the higher Reynolds number was used. The velocity profile was measured 10cm downstream from the entrance, which is the fully developed region. Figure 7 shows that the velocity profiles up to $Re=2100$ overlap each other very well, while the velocity profile at $Re=2900$ clearly deviates from others. Though more experiments are needed at Reynolds numbers between 2100 and 2900 to specify the critical Reynolds number, it seems the transition occurs in the range of $Re=2100\sim 2900$, which agrees with the conventional Re_{crit} in the macrochannel flow.

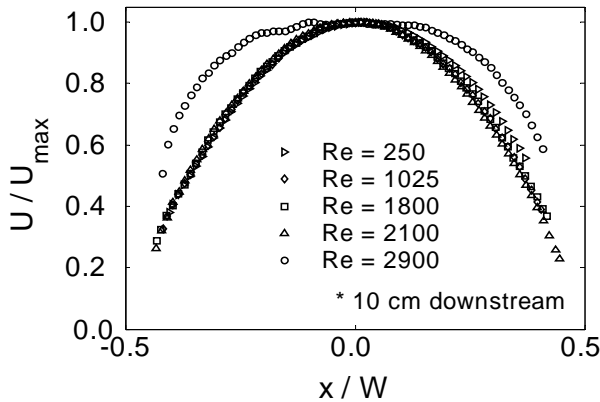


Fig. 7. Velocity profiles of the fully developed laminar flows compared to a higher Reynolds number.

The turbulence intensity was calculated to compare the turbulence strength at each Reynolds number.[26] From the vector fields at 10cm downstream, centerline velocities were extracted. The centerline velocity, $U_1(x_o, y, N)$, is the function of the axial direction coordinate, y , and the number of vector fields, N , where x_o and subscript 1 represent the center position and streamwise direction, respectively. Each case has $N (=100)$ consecutive vector fields and the velocity fluctuation, $u_1(x_o, y, N)$, was found by

$$u_1(x_o, y, N) = U_1(x_o, y, N) - \frac{1}{N} \sum_1^N U_1(x_o, y, N) \quad (6)$$

The turbulence intensity, $u_1^*(x_o, y)$, and the relative turbulence intensity then calculated, respectively, as

$$u_1^*(x_o, y) = \left[\frac{1}{N} \sum_1^N u_1^2(x_o, y, N) \right]^{1/2} \quad \text{and} \quad \frac{u_1^*(x_o, y)}{U_{avg}} \quad (7)$$

The spatially averaged relative turbulence intensity, $u_1^+(x_o)/U_{avg}$, is plotted in Fig. 8. As the Reynolds number increases, the relative turbulence intensity shows slight increase within less than 10% up to $Re=2100$ and a sudden increase occurs at $Re=2900$.

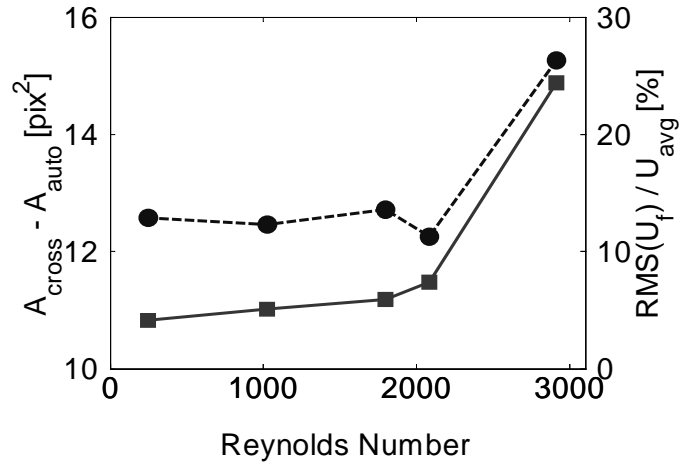


Fig. 8. Resemblance between the relative turbulence intensity (■) and the correlation peak broadening (●).

An close resemblance between the turbulence intensity and the correlation peak width broadening was observed. The correlation peak widths were calculated at $1/e$ height of the Gaussian function approximation, which is the twice of the standard deviation, of the normalized correlation peaks. The cross section area difference of the auto correlation and the cross correlation at $1/e$ height is plotted in Fig. 8 along with the relative turbulence intensity.

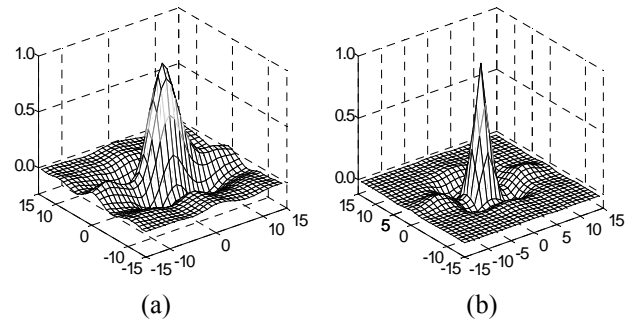


Fig. 9. Averaged correlation functions calculated at $Re=2900$ (a) Cross correlation peak. (b) Auto correlation peak

As in the flow field evaluation, the correlation peaks were evaluated using the averaged correlation algorithm and the μ PIV image filter.[18,23] Fig. 9(a) and (b) show the averaged cross and auto correlation functions and the correlation function peak broadening is clearly observed. Both correlation functions were calculated at $Re=2900$ and at $10cm$ downstream. The cross correlation function is evaluated from two image frames taken within $0.4\mu sec$ and the auto correlation function is found by self-correlating. Olsen and Adrian[21] found the correlation function peak broadening due to the Brownian motion of the seed particles. In the current study, because the error caused by the Brownian motion of the seed particles is extremely small(*e.g.* 0.02~0.06% for one particle), the correlation function peak broadening must be caused by other sources, likely turbulence. Similar to the recently developed temperature measurement based on the cross correlation analysis[22], the turbulence diffusion concept has been introduced to the peak broadening analysis. Further work must be done to make this technique quantitative, not just qualitative.

CONCLUSION

A $120mm$ long rectangular microchannel was fabricated with acrylic using conventional machining and adhesive layer bonding. The aspect ratio and the hydraulic diameter were 2.65 and $380\mu m$, respectively. The fabricated microchannel showed leak proof operation in the range of $Re=250-2900$. To avoid conventional machining limitations such as high tolerances on boundary dimensions and high surface roughness, microfabrication is recommended for future designs.

The effect of the typical microchannel inlet geometry on the entrance length for laminar flow was examined. The experimental results show the predevelopment due to the top and bottom walls in the reservoir upstream of the microchannel entrance significantly decrease the entrance length. The dimensionless entrance length found from the experiments shows that the entrance length is reduced about 45%. Assuming that the pressure entrance length shows the same dependence as the velocity entrance length on the altered inlet geometry of microfabricated planar microchannels, the pressure drop due to flow development should be lower than in flows with uniform inlet profile.

Laminar profiles were observed for $Re<2100$ while a transitional velocity profile was observed for $Re=2900$. Noting that the critical Reynolds number for the channel flow is 2300, the microchannel flow of the presented scale seems to follow the conventional theory of turbulence transition. The increase of the turbulence intensity at $Re=2900$ also showed that early transition did not occur in the current study.

A close resemblance between the correlation function peak broadening and the turbulence intensity was observed. From Fig. 8, the relative turbulence intensity increases to about 25% at $Re=2900$, while its value remains less than 10% in the rest of Reynolds numbers, so similarly does the cross section broadening of the correlation peak. To provide a functional form for this resemblance, further work will be needed.

ACKNOWLEDGMENTS

This work was supported by the Indiana 21st Century Research and Technology Fund.

One of the authors(I. Mudawar) is grateful for the support of the Office of Basic Energy Science of the U.S. Department of Energy(Award No. DE-FG02-93ER14394 A7)

REFERENCES

- [1] Tuckerman, D. B., Pease R. F. W., 1981, High-Performance Heat Sinking for VLSI, *IEEE Electron Device Letters*, Vol. EDL-2, no. 5, pp. 126-129
- [2] Han, L. S., 1983, "Hydrodynamic Entrance Lengths for Incompressible Laminar Flow in Rectangular Ducts", *J. of Applied Mechanics*, **27**, pp. 273-277
- [3] Wang, Y. L., and Longwell, P. A., 1964, "Laminar Flow in the Inlet Section of Parallel Plates", *AIChE J.*, **10**, pp. 323-329
- [4] Goldstein, R. J., Dreid, D. K., 1967, "Measurement of Laminar Flow Development in a Square Duct using a Laser-Doppler Flowmeter", *ASME J. of Applied Mechanics*, **34**, pp. 813-818
- [5] Sparrow, E. M., Hixon, C. W., and Shavit, G., 1967, "Experiments on Laminar Flow Development in Rectangular Ducts", *ASME J. of Basic Engineering*, **89**, pp. 116-124
- [6] Atkinson, B., Brocklebank, M. P., Card, C. C. H., and Smith, J. M., 1969, "Low Reynolds Number Developing Flows", *AIChE J.*, **15**, pp. 548-553
- [7] Fleming, D. P., and Sparrow, E. M., 1969, "Flow in the Hydrodynamic Entrance Region of Ducts of Arbitrary Cross Section", *ASME J. of Heat Transfer*, **91**, no. 3, pp. 345-354
- [8] Abarbanel, S., Bennett, S., Brandt, A., and Gillis, J., 1970, "Velocity Profiles of Flow at Low Reynolds Numbers", *ASME J. of Applied Mechanics*, **37**, pp. 2-4
- [9] Beavers G. S., Sparrow E. M., and Magnuson R. A., 1970, "Experiments on hydrodynamically developing flow in rectangular ducts of arbitrary aspect ratio", *International Journal of Heat & Mass Transfer*, **13**, no. 4, pp. 689-702
- [10] McDonald, J. W., Denny, V. E., and Mills, A. F., 1972, "Numerical Solutions of the Navier-Stokes Equations in Inlet Regions", *J. of Applied Mechanics*, **39**, no. 4, pp. 873-878
- [11] Sparrow, E. M., Anderson, C. E., 1977, "Effect of Upstream Flow Processes on Hydrodynamic Development in a Duct", *ASME J. of Fluids Engineering*, **99**, no. 3, pp. 556-560
- [12] Shah, R. K., 1978, "A Correlation for Laminar Hydrodynamic Entry Length Solutions for Circular and Noncircular Ducts", *ASME J. of Fluids Engineering*, **100**, no. 3, pp. 177-179
- [13] Wu, P. and Little, W. A., 1983, "Measurement of Friction Factors for the Flow of Gases in Very Fine Channels used for Microminiature Joule-Thomson Refrigerators", *Cryogenics*, **23**, pp. 273-277
- [14] Pfahler, J., Harley, J., Bau, H., Zemel, J. N., 1991, "Gas and Liquid Flow in Small Channels", *Micromechanical Sensors, Actuators, and Systems*, ASME, DSC, v. **32**, pp. 49-60
- [15] Peng, Z. F., Peterson, G. P., Wang, B. X., 1994, "Frictional Flow Characteristics of Water Flowing Through Rectangular Microchannels", *Experimental Heat Transfer*, **7**, pp. 249-264
- [16] Sharp, K. V., Adrian, R. J., Beebe, D. J., 2000, "Anomalous Transition to Turbulence in Microtubes", *MEMS-ASME*, **2**, pp. 461-466
- [17] Santiago, J. G., Wereley, S. T., Meinhart, C. D., Beebe, D. J., Adrian, R. J., 1998, "A Particle Image Velocimetry System for Microfluidics", *Experiments in Fluids*, **25**, pp. 316-319

- [18] Meinhart, C. D., Wereley, S. T., Santiago, J. G.(1999) A PIV Algorithm for Estimating Time-Averaged Velocity Fields, *Journal of Fluids Engineering*, v.122, 285-289
- [19] Wereley, S. T., Meinhart, C. D., Santiago, J. G., and Adrian, R. J., 1998, "Velocimetry for MEMS applications", *Micro-Electro-Mechanical Systems*, DSC. **66**, ASME, pp. 453-459
- [20] Meinhart, C. D., Wereley, S. T., and Gray, M. H. B., 2000, "Volume Illumination for Two-Dimensional Particle Image Velocimetry", *Meas. Sci. Technol.*, **11**, pp. 809-814
- [21] Olsen, M. G., and Adrian, R. J., 2000, "Brownian Motion and Correlation in Particle Image Velocimetry", *Optics and Laser Technology*, **32**, pp. 621-627
- [22] Wereley, S. T. and Hohreiter, V.P., 2002, "Simultaneous, Spatially-Resolved Temperature and Velocity Measurements Using Cross-Correlation PIV," paper 15.1, *Proceedings of the 11th International Symposium on the Application of Laser Techniques to Fluid Mechanics*, (Lisbon, Portugal), July 8-11.
- [23] Gui, L., Wereley, S. T., and Lee, S. Y., 2002, "Digital Filters for Reducing Background Noise in Micro PIV Measurements," paper 12.4, *Proceedings of the 11th International Symposium on the Application of Laser Techniques to Fluid Mechanics*, (Lisbon, Portugal), July 8-11.
- [24] Shah, R. K., and London, A. L., 1978, *Laminar Flow Forced Convection in Ducts - A Source Book for Compact Heat Exchanger Analytical Data*, Supplement 1 to *Advances in Heat Transfer Series*, Academic Press, New York.
- [25] Olson, R. M., and Wright, S. J., 1990, *Essentials of Engineering Fluid Mechanics*, Harper & Row, New York.
- [26] Tennekes, H., and Lumley, J. L., 1972, *A First Course in Turbulence*, The MIT Press, Cambridge.